# μ Control for Satellites Formation Flying

Yunjun Xu[1]; Norman Fitz-Coy[2]; Rick Lind[3]; and Andrew Tatsch[4]

**Abstract:** In this paper, a μ controller is designed for a satellite formation flying system around the Earth based on an uncertainty model derived from a nonlinear relative position equation. In this model, nonzero eccentricity and varying semimajor axis are included as parametric uncertainties. $J_2$ perturbation, atmospheric drag, and actuation and sensor noise are bounded by functional uncertainties. The μ controller design based on the nominal mission (an 800 km altitude circular reference orbit) is capable of achieving desired performance, is robust to uncertainties, and satisfies fuel consumption requirements even in a challenge nonnominal mission (a 0.1 eccentricity and 7,978 km semimajor axis elliptic reference orbit) with the same control gain. In this nonnominal mission, the designed μ controller is able to keep formation with almost the same level of the $\Delta V$ budget (43.86 m/s/year) as used in the nominal mission (39.65 m/s/year). For comparison, linear quadratic regulator (LQR) and sliding mode controllers (SMC) are developed and extensively tuned to get the same $\Delta V$ consumption as that of the designed μ controller for the nominal mission. However, as shown in the simulation, the designed linear robust controller (LQR) and nonlinear robust controller (SMC) have a serious $\Delta V$ consumption penalty (1.72 km/s/year for SMC) or are unstable (for LQR) in the nonnominal mission.

**DOI:** 10.1061/(ASCE)0893-1321(2007)20:1(10)

**CE Database subject headings:** Satellites; Dynamics; Models; Control systems.

## Introduction

Formation flying systems (FFS) have been investigated and proposed for military or nonmilitary services. Due to their potential advantages over the conventional large size monolithic satellite, such as the low cost, flexibility, improved observation efficiency, increased reliability, and enhanced survivability, many missions are considering the use of satellite or spacecraft FFS to achieve goals that are difficult for the conventional large-size single system. An ongoing FFS mission list includes the New Millennium Program (DS1, DS2, EO-1, EO-3, ST-5, and ST-6), microarcsecond X-ray imaging mission (MAXIM) (Luquette and Sanner 2003), terrestrial planet finder (TPF) (Luquette and Sanner 2003), Stellar Imager (Luquette and Sanner 2003), SPHERES (Miller et al. 2003), ACE (Dahl et al. 1999), TerraSAR-X/TanDEM-X [synthetic aperture radar (SAR)] (D' Amico et al. 2005), Gemini (Gill et al. 2001), and GRACE (Kirschner et al. 2004). The typical distance among space satellites in a formation ranges from 30 m to 200 km, with the control precision in a range from 1 m to 50 km.

[1]Assistant Professor, School of Aerospace and Mechanical Engineering, Univ. of Oklahoma, Norman, OK 73019. E-mail: yjxu@ou.edu

[2]Associate Professor, Mechanical and Aerospace Engineering, Univ. of Florida, Gainesville, FL 32611. E-mail: nfc@ufl.edu

[3]Assistant Professor, Mechanical and Aerospace Engineering, Univ. of Florida, Gainesville, FL 32611. E-mail: ricklind@ufl.edu

[4]Research Assistant, Mechanical and Aerospace Engineering, Univ. of Florida, Gainesville, FL 32611. E-mail: atatsch@ufl.edu

Note. Discussion open until June 1, 2007. Separate discussions must be submitted for individual papers. To extend the closing date by one month, a written request must be filed with the ASCE Managing Editor. The manuscript for this paper was submitted for review and possible publication on April 15, 2005; approved on November 18, 2005. This paper is part of the ***Journal of Aerospace Engineering***, Vol. 20, No. 1, January 1, 2007. ©ASCE, ISSN 0893-1321/2007/1-10–21/$25.00.

In relative dynamic models for FFS, the Clohessy-Wiltshire (CW) equation is most widely used (Redding and Adams 1989; Kapila et al. 1999; Robertson et al. 1999; Morton and Weininger 1999; Aorpimai et al. 1999; Vassar and Sherwood 1985; Sedwick et al. 1999; Yan et al. 2000; Yedavalli and Sparks 2000). Based on this linear model, Redding and Adams (1989) and Kapila et al. (1999) designed LQ controllers for a pulse-based thruster, whereas Robertson et al. (1999) implemented a PD controller with a thruster mapping. Sedwick et al. (1999) derived an analytical expression for an exact cancellation of differential $J_2$ for a satellite formation in a polar, circular orbit. Yan et al. (2000) designed a pulse-based control for the formation satellites' periodic motion which guarantees the global stability. Yedavalli and Sparks (2000) proposed a hybrid control scheme to achieve a balance between discrete control efforts and continuous dynamics performance. Ulybyshev (2003) designed a discrete LQR controller for an 800 km altitude Earth orbit formation mission with fuel consumption on the order of $\Delta V = 50$ m/s/year for formation satellites station keeping within a [20–40 km] control precision.

All the above-mentioned controllers are designed using the CW equation. However, the CW equation is a linear approximation of the real system, and does not contain atmospheric drag, high order harmonic terms, and uncertainties. Furthermore, the CW equation is only applicable in the near circular reference orbit case. Among these effects, higher order harmonic terms [especially $J_2$, which changes the orbit period, drifts the perigee, and changes the nodal precession rate (Alfriend et al. 2000)] and eccentricity are the dominant ones which affect the drifting of the CW equation. Therefore, mitigating the relative distance drift effects coming from $J_2$ and elliptic reference orbits have been investigated by many researchers.

Schweighart and Sedwick (2001) studied the effect of $J_2$ on the orbital elements, and a linearized $J_2$ form is added to the right of the CW equation. Yeh et al. (2000) designed a Lyapunov-type nonlinear controller for the $J_2$ perturbation rejection based on the CW equation; the $\Delta V$ budget is on the order of 100 m/s for only

180 h for a control precision of 1 km (4.8 km/s/year) in a low earth orbit FFS. Schaub and Alfriend (1999), Vadali et al. (2002, 1999), Schaub and Alfriend (2001, 2000), Alfriend et al. (2001), and Schaub et al. (2000) made significant contributions and published a series of papers that proposed a $J_2$ invariant model based on mean orbital elements, and derived the relationships between the relative position and velocity variables in the local frame and the orbital element differences. Two first-order (detailed information can be found in Schaub and Alfriend 1999) conditions are required to be satisfied that guarantee the drift rates of two satellites are equal on average under the $J_2$ perturbation. The basic idea is to constrain the drift rates, which are dependent on the mean semimajor axis, eccentricity, and inclination, of satellites so that the difference of drift rates and the secular drift can be minimized. It is found that the control effort required to overcome the $J_2$ perturbation is proportional to its inclination difference and the required $\Delta V$ is on the order of 50 m/s/year. However there are two limitations for $J_2$ invariant orbits. First, the two first-order constraints limit the selection of orbits, making FFS missions design, launching, and formation initialization inflexible. Second, the invariant is only on an average sense and the fuel consumption will increase if a precision or tight formation mission is pursued or a coupled attitude control is required. (In the future, useful FFS mission will require a cooperative pointing capability.) Except for the linear CW model, Pan and Kapila (2001) and Xu and Fitz-Coy (2003a,b) used a nonlinear relative position model with coupled attitude models derived from the gravitational gradient torque or cooperative pointing requirements. A higher computational cost associated with the nonlinear model propagation is still a disadvantage, although the current on-board computational capability has been increased significantly.

Since CW has an assumption of a near circular reference orbit, the eccentricity effects are also studied. Inalhan et al. (2002) described relative position motions for the case of an elliptic reference orbit instead of a circular reference orbit. In the noncircular case, the time dependence was replaced with the true anomaly dependence. Inalhan's paper focuses on developing a T-periodic solution, which has the satellites return to the initial relative states at the end of one orbital period. Another approach to evaluate an elliptic orbit reference case was provided by Schiff et al. (2000). This approach, however, is limited to nearly circular orbits as it is based on the CW equation.

In addition to the $J_2$ perturbation and elliptic reference orbits cases, uncertainty rejection techniques are also studied. Different kinds of controllers have been designed, which include Lyapunov-type control, such as the sliding mode control (Xu and Fitz-Coy 2003a,b; Lee and Cochran 1997) and the adaptive control (Pan and Kapila 2001; Gurfil et al. 2003). The uncertainties considered in these articles are mostly mass and inertia variations or functional uncertainties. Furthermore, optimal controls using Hamiltonia-Jacobi-Bellman methods (Beard and Hadaegh 1999; Campbell 2003; Wiesel 2003) are also proposed for path planning, optimization with constraints, and two-point boundary value problems in FFS reconfigurations.

The main contributions of this paper can be summarized in three areas:

An uncertainty model is derived from a nonlinear relative position model with eccentricity and semimajor axis variation considerations. The small eccentricity introduced into the model may come from an initial launch error, mission requirements, or misalignments. Even a very small eccentricity will change the linear system's open loop stability attributes. The semimajor axis of the orbit may also be required to change due to the formation reconfiguration. Therefore, robustness to eccentricities and semimajor axis is beneficial as opposed to only considering the changes in mass or inertia matrix properties. In this paper, the eccentricity uncertainty and semimajor axis variation are modeled as parametric uncertainties. Other perturbations, such as $J_2$ effects and atmospheric drag, are bounded by functional uncertainties. Also, noise associated with actuation and sensor systems are included.

A $\mu$ robust controller is designed capable of achieving desired performance, robustness, and fuel consumption requirements. For linear systems, linear quadratic regulator (LQR) and $H_\infty$ type controllers are normally formulated to guarantee robustness with respect to loop gains (Balas et al. 2001). For nonlinear systems, sliding mode is one of the commonly used controllers designed to guarantee stability when the system has functional uncertainties (Slotine and Li 1990). However, such robustness is sometimes conservative. $\mu$ is used to reduce the conservativeness of the controller by allowing the robustness measure to directly account for parametric uncertainties as well as functional uncertainties. Compared with adaptive and Lyapnov-type controllers, the $\mu$ controller designed has less computational cost and does not have an implicit dynamics inversion which may cancel the natural relative motion and increase the fuel consumption.

The method applied in this paper can be used to correct initial condition misalignment problems since there is no guarantee that the formation satellites are initially placed exactly into the desired orbit. In addition, this method can be used to precisely control the formation under the $J_2$ perturbation, sensor noise, and actuation noise with reasonable fuel consumptions (43.86 m/s/year) and has robustness against the nonzero eccentricity and different semimajor axis. The goal of the paper is to use one designed controller to control relative motions of the formation satellites under different mission profiles including circular and elliptic reference orbits together with different semimajor axes without a serious fuel consumption penalty. To show the unique feature of the proposed control method, a challenge mission is chosen for study. In the nominal mission, the reference orbit is assumed to be an 800 km altitude (7,178 km semimajor axis) circular orbit with a 35° inclination. The designed controller based on the nominal mission is to be used later in a mission with a reference orbit having a 7978 km semimajor axis, an eccentricity of 0.1, and a 35° inclination. The same designed controller is able to keep the formation without a fuel consumption penalty as used in the nominal system. However, as shown in the simulation, the designed (after extensive tuning) linear robust control (LQR) and nonlinear robust controller (SMC) based on the first mission have serious fuel consumption penalties or became unstable for the second mission.

In the next section, a linear model with parametric uncertainties (due to eccentricity and semimajor axis variations) is derived and the difference from the CW model is discussed. Then a $\mu$ controller is developed. For comparison purposes, a linear robust control (LQR) and a nonlinear robust controller (SMC) are also developed and extensively tuned in order to achieve the same level of fuel consumption as that of the designed $\mu$ controller. After that, simulations are presented showing that using the designed $\mu$ controller, the $\Delta V$ budget for a 1 year station keeping mission is less than 43.86 m/s for both missions. Finally, a conclusion is given.

## Dynamics Models

The FFS model can be simplified as a leader–follower pair as shown in Fig. 1. The nonlinear relative position model is pre-

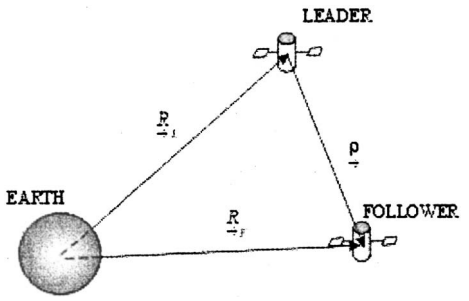


**Fig. 1.** Leader–follower pair

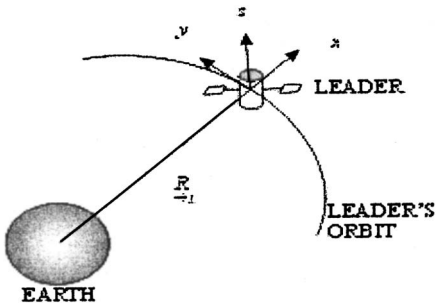


**Fig. 2.** LVLH coordinate system: (a) 7,178 km semimajor axis; (b) 7,978 km semimajor axis

sented in Eq. (1), which is expressed in the local horizontal local vertical frame (LVLH) as shown in Fig. 2 and includes exogenous effects such as control inputs, $J_2$ perturbations acceleration $\mathbf{a}_{J_2}$, and atmospheric drag acceleration $\mathbf{a}_{\text{drag}}$. $\tilde{\mu}$=gravitational constant of the Earth. $\mathbf{R}_L=[x_L,y_L,z_L]^T$ and $\mathbf{R}_F$=position vectors from the center of the Earth to the leader and follower, respectively, and $R_L$ and $R_F$=corresponding position magnitudes, $\boldsymbol{\rho}=[\rho_1,\rho_2,\rho_3]^T$ is the relative position vector from the leader to the follower satellite (i.e., $\boldsymbol{\rho}=\mathbf{R}_F-\mathbf{R}_L$). It is worth noting that the absolute position information for both satellites is not necessary for this model of the leader–follower pair; absolute position is only required for one of the two satellites. $\mathbf{u}$ is the control acceleration acting on the follower satellite and assumed to have control authorities in all three directions. $\boldsymbol{\omega}=[0,0,\dot{f}_L]^T$ and $\dot{\boldsymbol{\omega}}=[0,0,\ddot{f}_L]^T$ are angular velocity of the leader with true anomaly rate $\dot{f}_L$ and true anomaly acceleration $\ddot{f}_L$. The $J_2$ and atmospheric drag accelerations (Prussing and Conway 1993) are listed in Eqs. (2) and (3). In these equations, $J_2=1.08263\times10^{-3}$, $R_e$=6,378 km, and $m$=mass of a satellite. $\hat{\mathbf{e}}_r$ and $\hat{\mathbf{Z}}$=unit vectors in the radial direction of the follower satellite and $Z$ direction of the earth centered frame. For an orbital altitude above 500 km, the $J_2$ perturbation is the dominant one compared with the atmospheric drag. However, both are included in this paper for fidelity purposes

$$\ddot{\boldsymbol{\rho}}=-\dot{\boldsymbol{\omega}}\times\boldsymbol{\rho}-2\boldsymbol{\omega}\times\dot{\boldsymbol{\rho}}-\boldsymbol{\omega}\times(\boldsymbol{\omega}\times\boldsymbol{\rho})+\tilde{\mu}/R_L^3\mathbf{R}_L-\tilde{\mu}/R_F^3\mathbf{R}_F+\mathbf{u}+\mathbf{a}_{J_2}+\mathbf{a}_{\text{drag}} \tag{1}$$

$$\mathbf{a}_{J_2}=-\tilde{\mu}J_2R_e^2(3/(2R_f^4)-15Z^2/(2R_F^6))\hat{\mathbf{e}}_r-3\tilde{\mu}J_2R_e^2Z/(R_F^5)\hat{\mathbf{Z}} \tag{2}$$

$$\mathbf{a}_{\text{drag}}=-1/2(\rho C_DA/m)\|\mathbf{V}\|\mathbf{V} \tag{3}$$

The CW equation is derived based on the assumption that the reference orbit is a near circular orbit. Here we will derive a linear model without this assumption. In deriving this model, the atmospheric drag model and $J_2$ perturbation will be neglected and regarded as functional uncertainties. They will be added into the linear system together with the control input after the linear system is obtained. Thus neglecting the exogenous part of Eq. (1) and performing the Taylor series expansion of $\tilde{\mu}/R_F^3\mathbf{R}_F$ yield

$$(\tilde{\mu}/R_F^3)\mathbf{R}_F=(\tilde{\mu}/R_L^3)\mathbf{R}_L+\partial/\partial\mathbf{R}_L[(\tilde{\mu}/R_L^3\mathbf{R}_L)]\rho+o(\boldsymbol{\rho}^2) \tag{4}$$

$$\left[\frac{\partial}{\partial\mathbf{R}_L}\left(\frac{\tilde{\mu}}{R_L^3}\mathbf{R}_L\right)\right]=\frac{\tilde{\mu}}{R_L^5}\begin{bmatrix}R_L^2-3x_L^2 & -3x_Ly_L & -3x_Lz_L\\ -3x_Ly_L & R_L^2-3y_L^2 & -3y_Lz_L\\ -3x_Lz_L & -3y_Lz_L & R_L^2-3z_L^2\end{bmatrix} \tag{5}$$

Expressing Eq. (5) in the LVLH frame, the term can be simplified as shown in Eq. (6) by using $[x_L,y_L,z_L]^T=[R_L,0,0]^T$

$$\left[\frac{\partial}{\partial\mathbf{R}_L}\left(\frac{\tilde{\mu}}{R_L^3}\mathbf{R}_L\right)\right]=\frac{\tilde{\mu}}{R_L^3}\begin{bmatrix}-2 & 0 & 0\\ 0 & 1 & 0\\ 0 & 0 & 1\end{bmatrix} \tag{6}$$

Substituting Eqs. (4)–(6) into Eq. (1) and regarding all the others as high order and uncertainty terms, the linear model considering the eccentricity reference orbit is derived in Eq. (7), where $o(\boldsymbol{\rho}^2)$=high order term. If the reference orbit is circular and the higher order terms and perturbation terms are neglected, then the model Eq. (7) is the same as the CW equation shown in Eq. (8), where $n$ is defined as $\sqrt{\tilde{\mu}/a_{L0}^3}$ (a constant in the circular reference orbit case) and $R_L=a_{L0}$ ($a_{L0}$=nominal semimajor axis of the leader's orbit)

$$\begin{bmatrix}\dot{\boldsymbol{\rho}}\\ \ddot{\boldsymbol{\rho}}\end{bmatrix}=\begin{bmatrix}0 & 0 & 0 & 1 & 0 & 0\\ 0 & 0 & 0 & 0 & 1 & 0\\ 0 & 0 & 0 & 0 & 0 & 1\\ \dot{f}_L^2+2\tilde{\mu}/R_L^3 & \ddot{f}_L & 0 & 0 & 2\dot{f}_L & 0\\ -\ddot{f}_L & \dot{f}_L^2-\tilde{\mu}/R_L^3 & 0 & -2\dot{f}_L & 0 & 0\\ 0 & 0 & -\tilde{\mu}/R_L^3 & 0 & 0 & 0\end{bmatrix}\begin{bmatrix}\boldsymbol{\rho}\\ \dot{\boldsymbol{\rho}}\end{bmatrix}+\begin{bmatrix}0 & 0 & 0\\ 0 & 0 & 0\\ 0 & 0 & 0\\ 1 & 0 & 0\\ 0 & 1 & 0\\ 0 & 0 & 1\end{bmatrix}\mathbf{u}+\begin{bmatrix}0_{3\times3}\\ \mathbf{I}_{3\times3}O(\rho^2)\end{bmatrix} \tag{7}$$

$$\begin{bmatrix}\dot{\boldsymbol{\rho}}\\ \ddot{\boldsymbol{\rho}}\end{bmatrix}=\begin{bmatrix}0&0&0&1&0&0\\0&0&0&0&1&0\\0&0&0&0&0&1\\3n^2&0&0&0&2n&0\\0&0&0&-2n&0&0\\0&0&-n^2&0&0&0\end{bmatrix}\begin{bmatrix}\boldsymbol{\rho}\\ \dot{\boldsymbol{\rho}}\end{bmatrix}+\begin{bmatrix}0&0&0\\0&0&0\\0&0&0\\1&0&0\\0&1&0\\0&0&1\end{bmatrix}\mathbf{u} \tag{8}$$

The true anomaly rate (Inalhan et al. 2002; Bate et al. 1971; Chobotov 1996) and true anomaly accelerations are defined by Eqs. (9) and (10). Furthermore, these equations are used to propagate the true anomaly in the simulation of the elliptic reference orbit case. In these equations, $e_L$=eccentricity of the leader

$$\dot{f}_L=\frac{\sqrt{\tilde{\mu}a_L(1-e_L^2)}}{R_L^2} \tag{9}$$

$$\ddot{f}_L=\frac{-2\tilde{\mu}e_L(1+e_L\cos f_L)^3\sin f_L}{a_L^3(1-e_L^2)^3} \tag{10}$$

The linear dynamics model with eccentricity and semimajor axis variations can be rewritten as shown in Eq. (11), where the drag, $J_2$, and high order terms are all included, and subscript 0 denotes the nominal value. The actuation and sensor noises will be included in the controller designs and the simulations.

Comparing Eq. (11) with the CW model [Eq. (8)], the following statements can be made. First, if the eccentricity is zero with a nominal semimajor axis, they are identical. Second, the eigenvalues of the CW equation are all on the imaginary axis. Simulations have been done for all eccentricity cases ($e\in[0;1]$), and even an extremely small eccentricity will cause the open loop eigenvalues to be unstable, which may induce higher fuel consumptions in stabilizing the system. For example, when eccentricity is $10^{-2}$ and true anomaly is 1°, the eigenvalue of the open loop model has a pair of unstable eigenvalues to be $8.22\times10^{-7}\pm j1.96\times10^{-4}$, whereas in the zero eccentricity case, the eigenvalues are $[0,0,\pm j1.11\times10^{-3}]$. Therefore, the stability property is changed. In a real mission, there is a high probability that formation flying missions are initialized to have nonzero eccentricity. Based on this analysis, it is not difficult to see that the eccentricity needs to be modeled into the system when the control system is designed. Furthermore, as shown in Eq. (11) the semimajor axis affects the matrix elements

$$\begin{bmatrix}\dot{\boldsymbol{\rho}}\\ \ddot{\boldsymbol{\rho}}\end{bmatrix}=\begin{bmatrix}0&0&0&1&0&0\\0&0&0&0&1&0\\0&0&0&0&0&1\\3n^2\frac{(1+e_L\cos f_L)^3(3+e_L\cos f_L)}{3(1-e_L^2)^3}\left(\frac{a_{L0}}{a_L}\right)^3&\frac{-2\tilde{\mu}e_L(1+e_L\cos f_L)^3\sin f_L}{a_L^3(1-e_L^2)^3}&0&0&2n\sqrt{\frac{(1+e_L\cos f_L)^4}{(1-e_L^2)^3}}\left(\frac{a_{L0}}{a_L}\right)^{3/2}&0\\ \frac{-2\tilde{\mu}e_L(1+e_L\cos f_L)^3\sin f_L}{a_L^3(1-e_L^2)^3}&n^2\frac{e_L(1+e_L\cos f_L)^3\cos f_L}{(1-e_L^2)^3}\left(\frac{a_{L0}}{a_L}\right)^3&0&-2n\sqrt{\frac{(1+e_L\cos f_L)^4}{(1-e_L^2)^3}}\left(\frac{a_{L0}}{a_L}\right)^{3/2}&0&0\\ 0&0&-n^2\frac{(1+e_L\cos f_L)^3}{(1-e_L^2)^3}\left(\frac{a_{L0}}{a_L}\right)^3&0&0&0\end{bmatrix}\times\begin{bmatrix}\boldsymbol{\rho}\\ \dot{\boldsymbol{\rho}}\end{bmatrix}+\begin{bmatrix}0_{3\times3}\\ \mathbf{a}_{j_2}+\mathbf{a}_{\text{drag}}+\mathbf{u}+\mathbf{I}_{3\times3}o(\boldsymbol{\rho}^2)\end{bmatrix} \tag{11}$$

Therefore, in this paper, eccentricity and semimajor axis variations are modeled parametrically as shown in Eq. (12). The nominal model (CW equation) will be the equation without uncertainties $W_i\Delta, i\in1,\ldots,5$, where $\|\Delta\|\leqslant1$ and $W_i$=uncertainties boundary for the $i$th parameter. The actuation noise is modeled as random variables $\delta_1$ and the atmospheric drag, $J_2$ and other high order terms are modeled as random variables bounded by $\boldsymbol{\delta}_2$. Therefore, in this model, nonzero eccentricity, semimajor axis variations, drag, $J_2$, and actuation noise are all included. Sensor noise will be considered in the control synthesis discussed in the next section

$$\begin{bmatrix}\dot{\boldsymbol{\rho}}\\ \ddot{\boldsymbol{\rho}}\end{bmatrix}=\begin{bmatrix}0&0&0&1&0&0\\0&0&0&0&1&0\\0&0&0&0&0&1\\3n^2(1+W_i\Delta)&0+W_2\Delta&0&0&2n(1+W_5\Delta)&0\\0-W_2\Delta&0+W_3\Delta&0&-2n(1+W_5\Delta)&0&0\\0&0&-n^2(1+W_4\Delta)&0&0&0\end{bmatrix}\begin{bmatrix}\boldsymbol{\rho}\\ \dot{\boldsymbol{\rho}}\end{bmatrix}+\begin{bmatrix}0_{3\times3}\\ \delta_1\mathbf{u}+\boldsymbol{\delta}_2\end{bmatrix} \tag{12}$$

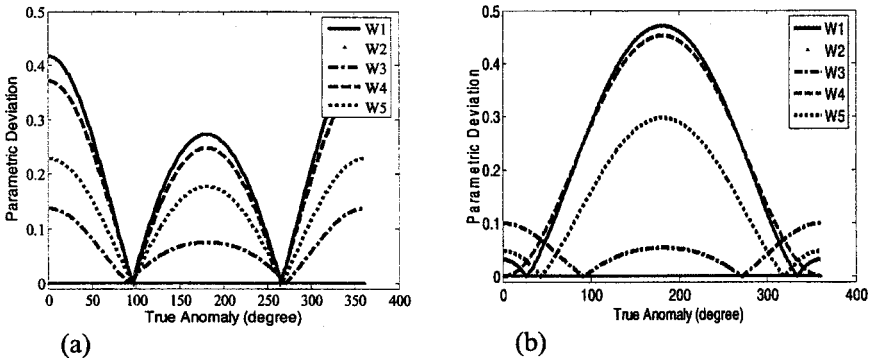


**Fig. 3.** Parametric absolute deviation due to nonzero eccentricity and different semimajor axis

In general, $J_2$ decreases the orbit altitude by 2% per orbit, and atmospheric drag in altitudes above 500 km is much less than the $J_2$ perturbation. Therefore, the $J_2$ and drag models are assumed to be bounded as 2% of the nominal system (CW model), and the actuation system and sensor noise is assumed to be 2%. As an example, for the eccentricity and semimajor axis parametric uncertainties, if the mission requires that the maximum eccentricity is bounded by 0.1 and the semimajor axis is varying between 7,178 and 7,978 km, the uncertainty magnitudes are calculated as $W_1=0.47, W_2=2.3\times10^{-7}, W_3=0.14, W_4=0.44,$ and $W_5=0.29$ as shown in Fig. 3(a and b). In Fig. 3, two extreme cases are shown for the semimajor axes to be 7,178 and 7,978 km.

## Control Synthesis

### *Control Objectives*

The μ controller will be designed to achieve desired performance, robust with respect to the nonzero eccentricity, semimajor axis change, actuation/sensor noise, atmospheric drag, $J_2$ effect, and other uncertainties. The gain and phase margins for the linear design need to be larger than 6 dB and 45°, and the μ value for the robust performance is less than one. The gain and phase margins are required to have proper stability margins. The three controllers' results are compared (μ, LQR, and SMC). For 1-year formation station keeping mission, $\Delta V$ is limited to be less than 50 m/s.

### μ *Synthesis*

First, the parametric uncertainty model is rewritten to a μ synthesis form. The nominal system is the CW equation. The eccentricity and semimajor axis are incorporated into the model as parametric uncertainties. Based on Eq. (12), three scalar equations in the relative acceleration part are rewritten as shown in Eqs. (13)–(15). The actuation noise $\delta_1$ and the high order term $\boldsymbol{\delta}_2$ are modeled as functional uncertainties which will be put into synthesis later

$$\ddot{\rho}_1 = 3n^2(1+W_1\Delta)\rho_1 + W_2\Delta\rho_2 + 2n(1+W_5\Delta)\dot{\rho}_2 + u_1$$

$$= 3n^2\rho_1 + 2n\dot{\rho}_2 + u_1 + (3n^2\rho_1)W_1\Delta + (\rho_2)W_2\Delta + (2n\dot{\rho}_2)W_5\Delta$$

$$\triangleq 3n^2\rho_1 + 2n\dot{\rho}_2 + u_1 + z_1\Delta + z_2\Delta + z_3\Delta$$

$$\triangleq 3n^2\rho_1 + 2n\dot{\rho}_2 + u_1 + w_1 + w_2 + w_3 \tag{13}$$

$$\ddot{\rho}_2 = -W_2\Delta\rho_1 + W_3\Delta\rho_2 - 2n(1+W_5\Delta)\dot{\rho}_1 + u_2$$

$$= -2n\dot{\rho}_1 + u_2 - \rho_1 W_2\Delta + \rho_2 W_3\Delta - 2n\dot{\rho}_1 W_5\Delta$$

$$\triangleq -2n\dot{\rho}_1 + u_2 + z_4\Delta + z_5\Delta + z_6\Delta$$

$$\triangleq -2n\dot{\rho}_1 + u_2 + w_4 + w_5 + w_6 \tag{14}$$

$$\ddot{\rho}_3 = -n^2(1+W_4\Delta)\rho_3 + u_3$$

$$= -n^2\rho_3 + u_3 - n^2\rho_3 W_4\Delta$$

$$\triangleq -n^2\rho_3 + u_3 + z_7\Delta$$

$$\triangleq -n^2\rho_3 + u_3 + w_7 \tag{15}$$

Within these equations, $z_1 \triangleq 3n^2\rho_1 W_1$, $z_2 \triangleq \rho_2 W_2$, $z_3 \triangleq 2n\dot{\rho}_2 W_5$, $z_4 \triangleq -\rho_1 W_2$, $z_5 \triangleq \rho_2 W_3$, $Z_6 \triangleq -2n\dot{\rho}_1 W_5$, and $z_7 \triangleq -n^2\rho_3 W_4$. $z_i$, $i \in [1,7]$=signals from the open loop block to the uncertainty block. $w_i \triangleq z_i\Delta$, $i \in [1,7]$ are inputs from the uncertainty block to the open loop block.

The input–output relation for the open loop is shown in Fig. 4. $u_i$, $i \in [1,3]$, is the control and $y_i$, $i \in [1,6]$ is composed of relative position and velocity. $w_i$ and $z_i$, $i \in [1,7]$ are the inputs and outputs of the parametric uncertainties block. Without noise and other functional uncertainties, the system is written in a state

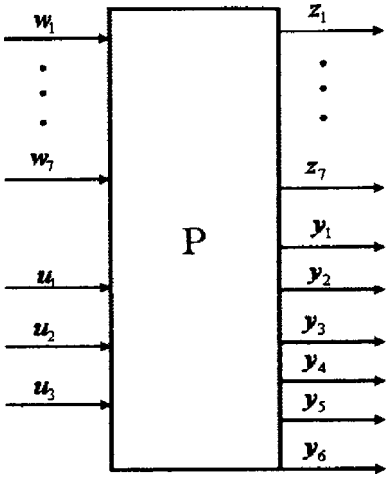


**Fig. 4.** Open-loop model with parametric uncertainty

space form as shown in Eq. (16) including states $[\boldsymbol{\rho}^T, \dot{\boldsymbol{\rho}}^T]^T \in \mathbb{R}^{6\times 1}$, exogenous signals $[\mathbf{w}^T, \mathbf{u}^T]^T \in \mathbb{R}^{10\times 1}$, uncertainty input signals $\mathbf{z} \in \mathbb{R}^{7\times 1}$, and output signals $\mathbf{y} \in \mathbb{R}^{6\times 1}$

$$P = \begin{bmatrix}
0 & 0 & 0 & 1 & 0 & 0 & 0 & 0 & 0 & 0 & 0 & 0 & 0 & 0 & 0 & 0 \\
0 & 0 & 0 & 0 & 1 & 0 & 0 & 0 & 0 & 0 & 0 & 0 & 0 & 0 & 0 & 0 \\
0 & 0 & 0 & 0 & 0 & 1 & 0 & 0 & 0 & 0 & 0 & 0 & 0 & 0 & 0 & 0 \\
3n^2 & 0 & 0 & 0 & 2n & 0 & 1 & 1 & 1 & 0 & 0 & 0 & 0 & 1 & 0 & 0 \\
0 & 0 & 0 & -2n & 0 & 0 & 0 & 0 & 0 & 1 & 1 & 1 & 0 & 0 & 1 & 0 \\
0 & 0 & -n^2 & 0 & 0 & 0 & 0 & 0 & 0 & 0 & 0 & 0 & 1 & 0 & 0 & 1 \\
3n^2W_1 & 0 & 0 & 0 & 0 & 0 & 0 & 0 & 0 & 0 & 0 & 0 & 0 & 0 & 0 & 0 \\
0 & W_2 & 0 & 0 & 0 & 0 & 0 & 0 & 0 & 0 & 0 & 0 & 0 & 0 & 0 & 0 \\
0 & 0 & 0 & 0 & 2nW_5 & 0 & 0 & 0 & 0 & 0 & 0 & 0 & 0 & 0 & 0 & 0 \\
-W_2 & 0 & 0 & 0 & 0 & 0 & 0 & 0 & 0 & 0 & 0 & 0 & 0 & 0 & 0 & 0 \\
0 & W_3 & 0 & 0 & 0 & 0 & 0 & 0 & 0 & 0 & 0 & 0 & 0 & 0 & 0 & 0 \\
0 & 0 & 0 & -2nW_5 & 0 & 0 & 0 & 0 & 0 & 0 & 0 & 0 & 0 & 0 & 0 & 0 \\
0 & 0 & -n^2W_4 & 0 & 0 & 0 & 0 & 0 & 0 & 0 & 0 & 0 & 0 & 0 & 0 & 0 \\
1 & 0 & 0 & 0 & 0 & 0 & 0 & 0 & 0 & 0 & 0 & 0 & 0 & 0 & 0 & 0 \\
0 & 1 & 0 & 0 & 0 & 0 & 0 & 0 & 0 & 0 & 0 & 0 & 0 & 0 & 0 & 0 \\
0 & 0 & 1 & 0 & 0 & 0 & 0 & 0 & 0 & 0 & 0 & 0 & 0 & 0 & 0 & 0 \\
0 & 0 & 0 & 1 & 0 & 0 & 0 & 0 & 0 & 0 & 0 & 0 & 0 & 0 & 0 & 0 \\
0 & 0 & 0 & 0 & 1 & 0 & 0 & 0 & 0 & 0 & 0 & 0 & 0 & 0 & 0 & 0 \\
0 & 0 & 0 & 0 & 0 & 1 & 0 & 0 & 0 & 0 & 0 & 0 & 0 & 0 & 0 & 0
\end{bmatrix} = \begin{bmatrix} \mathbf{A}_{6\times 6} & \mathbf{B}_{6\times 10} \\ \mathbf{C}_{13\times 6} & \mathbf{D}_{13\times 10} \end{bmatrix} \tag{16}$$

In Fig. 5, the synthesis model is shown, where the $(z_i, w_i)$, $i \in [1,7]$ shows the parametric uncertainty relation and $(z_i, w_i)$, $i \in [8,16]$ denotes the functional uncertainties associated with $J_2$, atmospheric drag, and actuation uncertainties. $\mathbf{W}_n$ is the noise matrix, $\mathbf{r} \in \mathbb{R}^{6\times 1}$=command for the relative states, $\mathbf{u} \in \mathbb{R}^{3\times 1}$=control input. The weighting function for the performance and control efforts are selected as $\mathbf{W}_{\text{perf}}=[0.1, 0.01, 0.1, 0.1, 0.01, 0.1][s/(s+1)]\mathbf{I}_{6\times 6}$ and $\mathbf{W}_u=\mathbf{I}_{3\times 3}$, respectively. Because the D-K iteration (Balas et al. 2001) usually gives very high order controllers, Hankel balanced model reduction is used to reduce the controller's order.

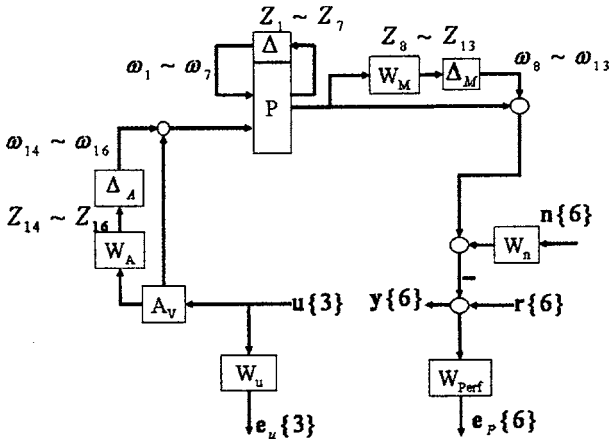


**Fig. 5.** Open-loop synthesis model

### *Robust Analysis*

The gain and phase margins of the μ controller based on the linear model are listed in Table 1. It is shown that the gain and phase margins of the μ satisfy the 6 dB and 45° conventional robustness requirements.

Nominal performance (NP), robust stability (RS), and robust performance (RP) are calculated as shown in Table 2 using μ theory for the μ controller. As shown in Table 2, all the values calculated by μ are less than one. Therefore, μ controller is capable of stabilizing the system and achieving the desired performance even under the predefined maximum uncertain system.

## LQR and SMC

For comparison, one linear robust controller (LQR) and one nonlinear robust controller (SMC) are shown here briefly. The detailed information can be found in Ulybyshev (1998), Lee and

**Table 1.** Gain and Phase Margins

| Controller | Gain margin (dB) | Phase margin (degrees) |
|---|---|---|
| μ | 6.04 | 57.52 |

**Table 2.** NP, RS, and RP

| Controller | NP | RS | RP |
|---|---|---|---|
| μ | 0.413 | 0.9371 | 0.9640 |

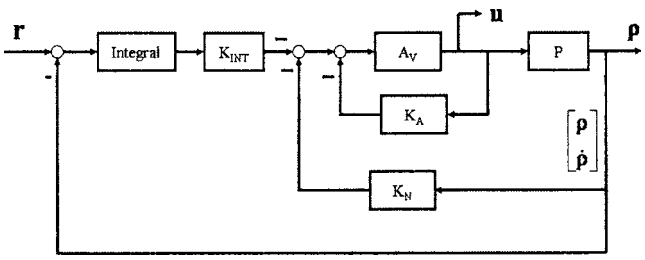


**Fig. 6.** LQR synthesis

Cochran (1997), and Soltine and Li (1990). Time response and fuel consumptions for a 1-year mission will be compared with the μ controller developed previously.

### LQR Synthesis

LQR controller is designed as shown in Fig. 6 and the LQ tracking states are $[\boldsymbol{\rho}^T, \dot{\boldsymbol{\rho}}^T, \int \mathbf{e}^T dt]^T \in \mathbb{R}^{12\times 1}$ where the error signal is the command signal minus the relative position state: $\mathbf{e}=\mathbf{r}-\mathbf{p}$. The weighting function used in finding feedback gains are listed in Eqs. (17) and (18). The weighting function $\mathbf{Q}$ is heavily weighted on the error signal as the controller is used to drive the error to zero. In order to achieve the same level of fuel consumption as the designed μ and sliding model controllers, an extremely high weighting function is in the $\mathbf{R}$ matrix

$$\mathbf{Q} = \begin{bmatrix} 10^{-20}\mathbf{I}_{9\times 9} & \mathbf{0}_{9\times 3} \\ \mathbf{0}_{3\times 9} & 10^{4}\mathbf{I}_{3\times 3} \end{bmatrix} \tag{17}$$

$$\mathbf{R}\begin{bmatrix} 10^{30} & 0 & 0 \\ 0 & 10^{30} & 0 \\ 0 & 0 & 10^{25} \end{bmatrix} \tag{18}$$

### SMC and Parametric Optimization

As an example of a nonlinear robust controller, a sliding mode control is designed based on the nonlinear model Eq. (1) where atmospheric drag and $J_2$ effect are regarded deterministically. The state function $\mathbf{f}$ [Eq. (19)] takes into account the nonzero eccentricity and semimajor axis variation. $\|\mathbf{f}_i - \hat{\mathbf{f}}_i\| \leq \mathbf{F}_i \in \mathbb{R}^{3\times 1}$, $i \in [1,2,3]$, where $\hat{\mathbf{f}}$ represents the predicted function. The sensor noise is modeled as random signals, and the actuation uncertainty is modeled as $\mathbf{B}=(1+\Delta_{ii})\hat{\mathbf{B}}$, $|\Delta_{ii}| \leq D_{ii}=2\%$. $\tilde{x}_i = x_i - r_i$ are error signal. The sliding mode controller is designed in Eq. (20). The sliding surface function and the boundary layer function are listed in Eqs. (21) and (22). In order to reduce the chattering phenomena associated with the signum function in the sliding model, the boundary function is used to replace the signum function with the compromise in the control precision. The caret denotes the predicted model. For consistency, 2% noise is assumed in the simulation. $\rho_{ri}^{(n_i-1)} \triangleq \rho_{di}^{(n_i-1)} - \lambda_i^{n_i-1}\tilde{\rho}_i$, $i=1,2,3$, and $\mathbf{K}\,\mathrm{sgn}(\mathbf{s}) \triangleq [K_i\,\mathrm{sgn}(s_i)]_{i=1,2,3}$. For the Lyapunov stability, $\lambda_i$ needs to be larger than zero, and $k_i$ is required to satisfy Eq. (23), where $\eta_i > 0$

$$\mathbf{f} = -\dot{\boldsymbol{\omega}} \times \boldsymbol{\rho} - 2\boldsymbol{\omega} \times \dot{\boldsymbol{\rho}} - \boldsymbol{\omega} \times (\boldsymbol{\omega} \times \boldsymbol{\rho}) + \tilde{\mu}/R_L^3 \mathbf{R}_L - \tilde{\mu}/R_F^3 \mathbf{R}_F + \mathbf{a}_{J_2} + \mathbf{a}_{\text{drag}} \tag{19}$$

$$\mathbf{u} = \hat{\mathbf{B}}^{-1}[\dot{\mathbf{x}}_r - \hat{\mathbf{f}} - \mathbf{K}\,\mathrm{sgn}(\mathbf{s})] \tag{20}$$

**Table 3.** GA Parameters Used

| Parameter | Data | Parameter | Physical meaning |
|---|---|---|---|
| Number of parameters | 18 | Number of generation | 20 |
| Bit length | 40 | Probability of crossover | 0.9 |
| Population size | 20 | Probability of mutation | 0.05 |

$$s_i = \left(\frac{d}{dt} + \lambda_i\right)\tilde{x}_i = \dot{x}_i - \dot{x}_{ri} \tag{21}$$

$$\mathrm{sgn}(s_i) \Rightarrow \mathrm{sat}(s_i/\varepsilon_i) = \begin{cases} \mathrm{sgn}(s_i) & s_i \geq 1 \\ s_i/\varepsilon_i & s_i < 1 \end{cases} \quad i = 1,2,\ldots,3 \tag{22}$$

$$(1 - D_{ii})k_i + \sum_{j\neq i} D_{ij}k_j = F_i + \sum_{j=1}^{n} D_{ij}|\dot{x}_{ri} - \hat{f}_j| + \eta_i \quad i,j = 1,2,3 \tag{23}$$

In order to achieve minimum fuel consumption, a genetic algorithm (Xu and Fitz-Coy 2003a,b) is used to select controllers' parameters to minimize the quadratic performance index as shown in Eq. (24). Because fuel consumption is a primary concern, the weighting matrix $\mathbf{R}$ is selected to be $\mathbf{R}=10^6\mathbf{Q}$. The genetic algorithm parameters are listed in Table 3

$$j = \frac{1}{2}\int_0^f (\tilde{\mathbf{x}}^T\mathbf{Q}\tilde{\mathbf{x}} + \mathbf{u}^T\mathbf{R}\mathbf{u})dt \tag{24}$$

## Simulation Results

In this section, the designed μ controller is tested in the missions as follows. With a working frequency of 1 Hz, a challenge mission is chosen for studying in this paper to show the strength of the proposed control method. The ode45 function in MATLAB is used for numerical integrations. The station keeping problem is studied and command $\mathbf{r}$ is the desired relative position between the leader and the follower satellites.

In order to compare the simulation results with other literature, first, a circular reference orbit case is simulated with drag, the $J_2$ perturbation, higher order terms, actuation, and sensor noise. The model used in this case is nonlinear. Initially, the leader is in the circular orbit with an altitude of 800 km. The follower is in circular orbits with the same altitude, but with a 0.1° true longitude behind the leader. The inclination of these two satellites' orbit is 35°. The thruster and sensor systems all have 2% random noise. This represents a typical formation keeping problem. In the literature [Ulybyshev (1998); Schaub and Alfriend (1999, 2000, 2001)] a reasonable $\Delta V$ consumed for formation station keeping is normally in the range of 50–100 m/s per year.

Second, a challenge elliptic reference orbit case is simulated to demonstrate the robustness of the designed μ controller. Both the leader and followers have 0.1 eccentricities and 7,978 km semimajor axis. The leader is in 35° inclination orbit and the followers have a 0.05° true longitude behind the leader. The thruster and sensor systems all have 2% random noise.

### Circular Reference Orbit

Figs. 7–9 show the relative position error in the LVLH coordinate system. In order to achieve the same level of $\Delta V$ budget, extensive tuning has been conducted for the LQR and SMC. As can be seen from the relative position error figure, the $\mu$ and SMC controllers have much higher control precision than that of LQR, which can also be seen from Table 4.

Figs. 10–12, give the control commands in the LVLH coordinate system. The oscillation in the $\mu$ controller is due to the quasiperiodic properties of the $J_2$ variation, whereas the oscillation in the SMC is due to the saturation level in the sliding surface. Further, the 2% noise can be seen in these figures, e.g., the LQR case.

### Elliptic Reference Orbit

The relative position errors are shown in Figs. 13–15. It is demonstrated that for this challenge mission the designed $\mu$ controller can achieve a much better control precision (70 m) than that of SMC (on the order of 3 km). The control commands for the three controllers are shown in Figs. 16–18. The LQR controller is unstable for this simulated mission. There are several reasons for the better performance in $\mu$ controller. First, the LQR and SMC are robust to functional uncertainties, and compared with $\mu$ controller, they are conservative. Second, the $\mu$ controller is designed considering both robustness and performance, whereas SMC only considers the stability under uncertainty cases. Note that the LQR synthesis is only tracking the relative position, whereas SMC and $\mu$ controllers are tracking both the velocity and position. This is due to the fact that the controllability matrix in LQR synthesis only has a rank 3. Therefore only three states can be tracked in this LQR synthesis.

In order to get a precision managed pointing capability for the formation (such as MAXIM), maintaining a precision orbit is important. The control precision of the simulations is shown in Table 4, where the largest steady state errors among all three directions are shown, which satisfies the requirement of millimeter level control precision in the nominal mission. In reality, this precision control may not be possible to achieve; however, the controller designed here demonstrates the precision capability if very precise sensors and thrusters are provided.

Note that theoretically, all the controllers should be able to achieve the same performance. However, extensive tuning of the parameters will not guarantee that all the methods could achieve the same results and here, the $\mu$ gives much better results than those of LQR and SMC.

### Fuel Consumption

The fuel consumptions ($\Delta V$) calculated for each simulation are shown in Table 5 for the two simulation cases. Here the annual $\Delta V$ is calculated based on the average budget obtained from the 15 h simulation. In the circular reference orbit, all three methods require a similar $\Delta V$ budget for a 1 year station keeping mission. In this table, it can be seen that using the $\mu$ controller, both these two missions' $\Delta V$ is less than 50 m/s/year, whereas, if SMC is

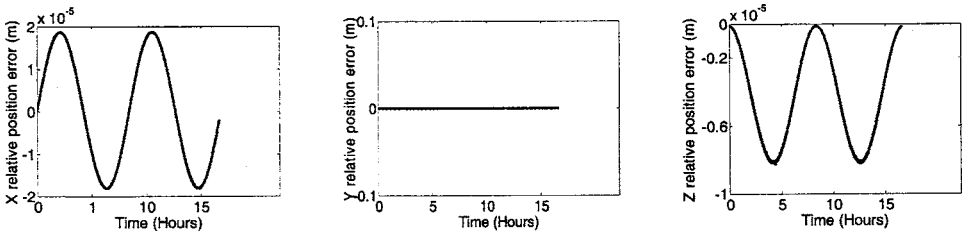


**Fig. 7.** Relative position error in the circular reference orbit case ($\mu$)

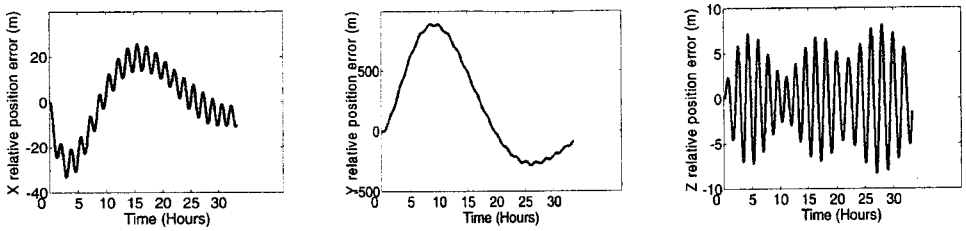


**Fig. 8.** Relative position error in the circular reference orbit case (LQR)

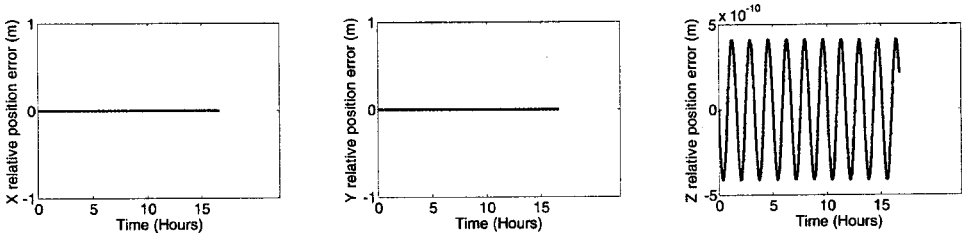


**Fig. 9.** Relative position error in the circular reference orbit case (SMC)

**Table 4.** Steady State Errors

| Controller | Circular nonlinear orbit | Nonlinear elliptic orbit |
|---|---|---|
| $\mu$ | $10^{-2}$ mm | 70 m |
| LQR | 0.01–0.8 km | 1–5 km (unstable) |
| SMC | $10^{-7}$ mm | 3 km |

used, the second mission's $\Delta V$ is too high. Compared to the SMC controller, the $\mu$ controller has less computational cost and does not have implicit dynamics inversion which needs precise knowledge of the dynamics model and may cancel the natural relative motion and increase the fuel consumption. The $\Delta V$ used in the SMC (1.72 km/s/year) for the second mission is similar to the reference (Yeh et al. 2000) (4.8 km/s/year), which is reasonable because the sliding mode control is based on Lyapunov theory.

Based on the comparison in control precision, stability, and fuel consumption, it can be seen that the designed $\mu$ controller has a much better performance.

## Conclusion

In this paper, an uncertainty model with the nonzero eccentricity and varying semimajor axis consideration is derived based on the nonlinear relative position model. Because even a very small eccentricity will change the linear system's open loop stability attributes, the eccentricity and semimajor axis variations are modeled into parametric uncertainties. Furthermore, $J_2$ effects and atmospheric drag, actuation, and sensor noise are bounded by functional uncertainties. A $\mu$ robust controller is designed capable of achieving desired performance, robustness to uncertainties, and fuel consumption requirement. For comparison, LQR and sliding mode controllers are developed and extensively tuned to get the same order of $\Delta V$ budget as that of the designed $\mu$ controller. To illustrate the advantages of the proposed control method, a challenge mission is chosen for analysis. In the nominal mission, the reference orbit is assumed to be an 800 km altitude (7,178 km semimajor axis) circular orbit with a 35° inclination. The de-

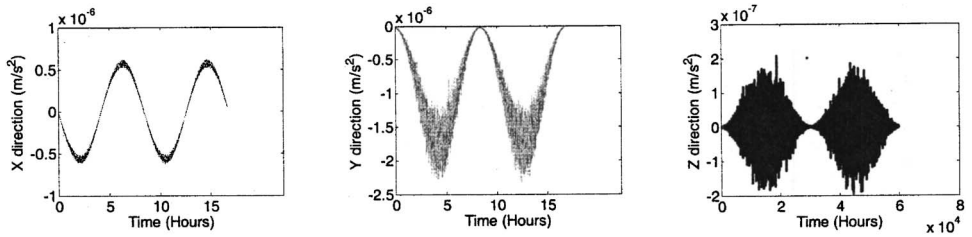


**Fig. 10.** Control accelerations in the circular reference orbit ($\mu$)

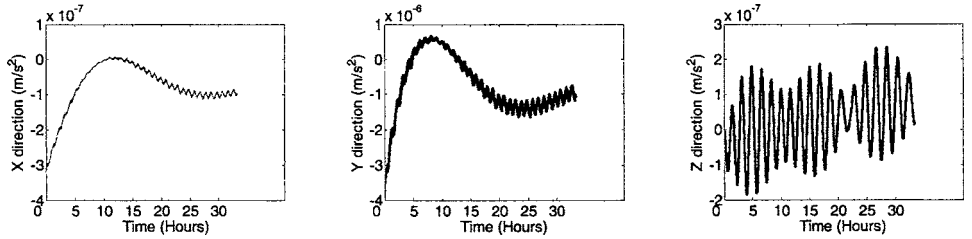


**Fig. 11.** Control accelerations in the circular reference orbit (LQR)

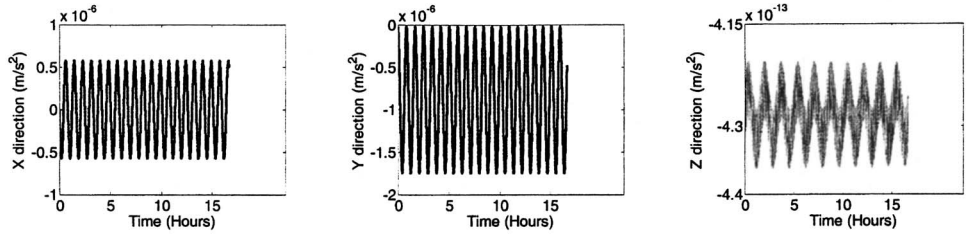


**Fig. 12.** Control accelerations in the circular reference orbit (SMC)

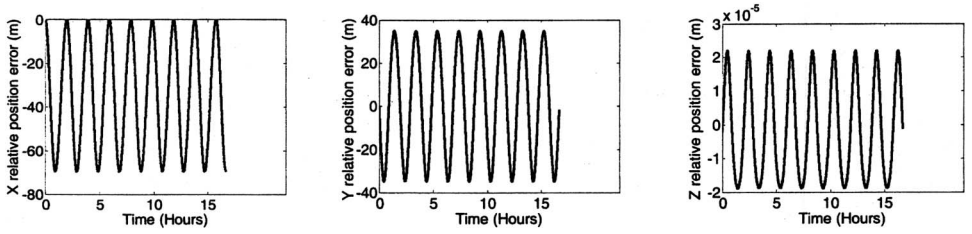


**Fig. 13.** Relative position error in the elliptic reference orbit case ($\mu$)

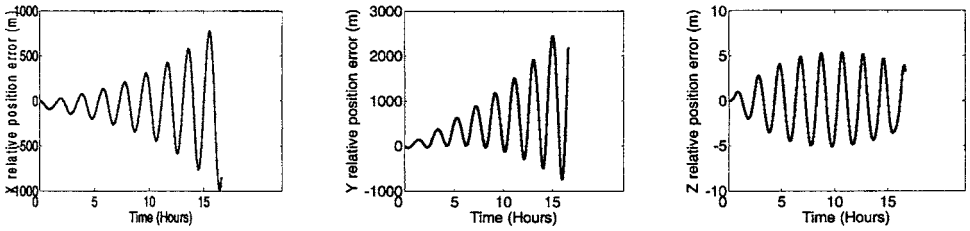


**Fig. 14.** Relative position error in the elliptic reference orbit case (LQR, unstable)

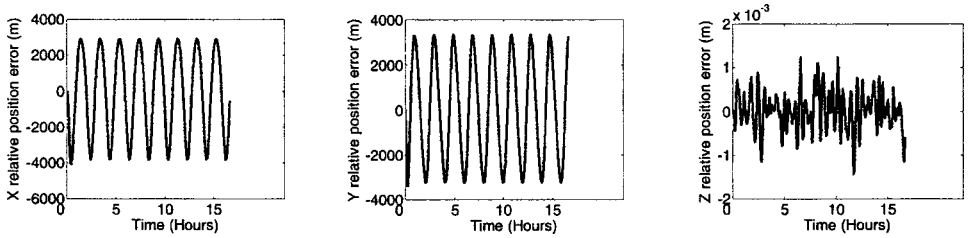


**Fig. 15.** Relative position error in the elliptic reference orbit case (SMC)

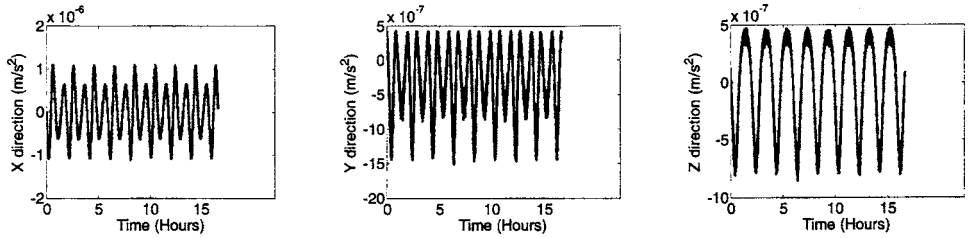


**Fig. 16.** Control accelerations in the elliptic reference orbit ($\mu$)

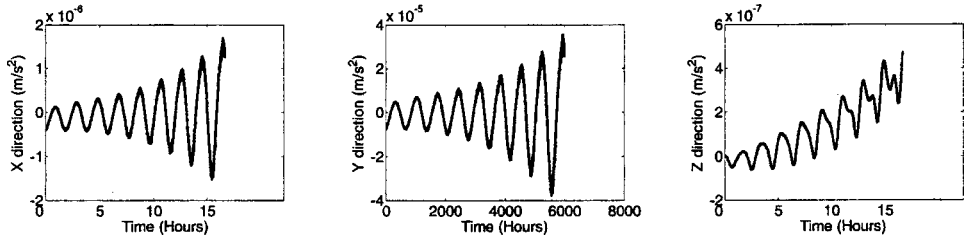


**Fig. 17.** Control accelerations in the elliptic reference orbit (LQR, unstable)

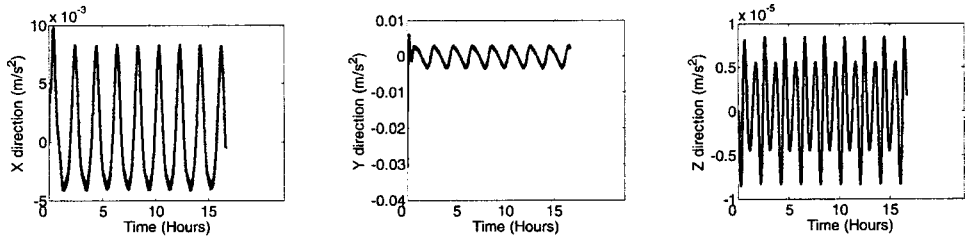


**Fig. 18.** Control accelerations in the elliptic reference orbit (SMC)

**Table 5.** Fuel Consumption per Year

| Controller | Nonlinear circular orbit (m/s) | Nonlinear elliptic orbit |
|---|---|---|
| $\mu$ | 39.65 | 43.86 m/s |
| LQR | 34.32 | 316 m/s (unstable) |
| SMC | 38.76 | 1.72 km/s (too high) |

signed controller based on the nominal mission is planned to be used later in a mission with a reference orbit having a 7,978 km semimajor axis, an eccentricity equals 0.1, and a 35° inclination. The same designed $\mu$ controller is able to keep the formation with almost the same fuel consumption (43.86 m/s/year) as used in the nominal system (39.65 m/s/year). However, as shown in the simulation, the designed (after extensive tuning) linear robust control (LQR) and nonlinear robust controller (SMC) have either serious fuel consumption penalties (1.72 km/s/year for SMC) or are unstable (LQR).

## Notation

*The following symbols are used in this paper:*

$A$ = cross-sectional area of satellites;
$\mathbf{a}$ = acceleration;
$C_D$ = drag coefficient;
$e$ = eccentricity;
$\hat{\mathbf{e}}_r$ = unit vector in the radial direction;
$f$ = true anomaly;
$J_2$ = $J_2$ perturbation coefficient;
$m$ = mass of a satellite
$n$ = mean motion of orbits;
$\mathbf{R}$ = absolute position vector;
$R$ = magnitude of the absolute position vector;
$\mathbf{r}$ = commands;
$\mathbf{s}$ = sliding mode surface;
$\mathbf{u}$ = normalized force with respect to mass;
$\mathbf{x}$ = states $[x;y;z]^T$;
$\hat{\mathbf{Z}}$ = $z$-direction in the Earth centered frame;
$\Delta V$ = fuel consumption budget;
$\tilde{\mu}$ = gravitational coefficient;
$\boldsymbol{\rho}$ = relative position vector;
$\rho$ = atmospheric density; and
$\boldsymbol{\omega}$ = angular velocity;

### *Subscripts*

drag = atmospheric drag effect;
$e$ = Earth;
$F$ = follower satellite;
$J_2$ = $J_2$ effect;
$L$ = leader satellite;
$r$ = radial direction; and
0 = nominal value.

### *Superscript*

$T$ = vector or matrix transpose.

## References


Alfriend, K. T., Schaub, H., and Gim, D. (2000). "Gravitational perturbations, nonlinearity and circular orbit assumption effects on formation flying control strategies." *AAS Rocky Mountain Guidance and Control Conf.*, Breckenridge, Colo.

Alfriend, K. T., Vadali, S. R., and Schaub, H. (2001). "Formation flying satellites: Control by an astrodynamicist." *Celest. Mech. Dyn. Astron.*, 81(1–2), 57–62.

Aorpimai, M., Palmer, P., and Curel, A. (1999). "Phase acquisition and formation keeping of a new power consumption monitoring satellite constellation." *13th Annual AIAA/USU Conf. on Small Satellite*, *SSC-99-VI-2*, Logan, Utah.

Balas, G. J., Doyle, J. C., Glover, K., Packard, A., and Smith, R. (2001). *$\mu$ analysis and synthesis toolbox for use with MATLAB*, The MathWorks, Natick, Mass., 111–124.

Bate, R. R., Mueller, D. D., and White, J. E. (1971). *Fundamentals of astrodynamics*, Dover, New York, 20, 25–33, 212–222, 396–412.

Beard, R. W., and Hadaegh, F. Y. (1999). "Finite thrust control for satellite formation flying with state constraints." *Proc., American Control Conf.*, San Diego, 4383–4387.

Campbell, M. E. (2003). "Planning algorithm for multiple satellite clusters." *J. Guid. Control Dyn.*, 26(5), 770–780.

Chobotov, V. A. (1996). *Orbital mechanics*, 2nd Ed., AIAA Educational Series, AIAA, Reston, Va., 155–158, 162–164, 168–181.

Dahl, H., Eliuk, W., Rumbold, G., and Shelly, R. (1999). "ACE-A Canadian small science satellite mission." *13th AIAA/USU Conf. on Small Satellites, SSC99-V-7*, Logan, Utah.

D'Amico, S., Montenbruck, O., Arbinger, C., and Fiedler, H. (2005). "Formation flying concept for close remote sensing satellites." *15th AAS/AIAA Space Flight Mechanics Meeting*, Cooper Mountain, Colo.

Gill, E., Steckling, M., and Butz, P. (2001). "Gemini: A milestone towards autonomous formation flying." *ESA Workshop on On-Board Autonomy*, ESTEC, Noordwijk, The Netherlands.

Gurfil, P., Idan, M., and Kasdin, N. J. (2003). "Adaptive neural control of deep-space formation flying." *J. Guid. Control Dyn.*, 26(3), 491–501.

Inalhan, G., Tillerson, M., and How, J. P. (2002). "Relative dynamics and control of spacecraft formations in eccentric orbits." *J. Guid. Control Dyn.*, 25(1), 43–60.

Kapila, V., Sparks, A. G., Buffington, J. M., and Yan, Q. (1999). "Spacecraft formation flying: Dynamics and control." *Proc., American Control Conf.*, Calif.

Kirschner, M., Montenbruck, O., and Amico, S. D. (2004). "Safe switching of the grace formation using an eccentricity/inclination vector separation." *18th Int. Symp. on Space Flight Dynamics*, Munich, Germany.

Lee, S., and Cochran, J. E. (1997). "Orbital maneuvers via feedback linearization and bang-bang control." *J. Guid. Control Dyn.*, 20(1), 104–110.

Luquette, R. J., and Sanner, R. M. (2003). "A nonlinear, six-degree of freedom, precision formation control algorithm, based on restricted three body dynamics." *26th Annual AAS Guidance and Control Conf.*, Breckenridge, Colo.

Miller, D. W., Kong, E. M. C., and Saenz-Otero, A. (2003). "Overview of the SPHERES autonomous rendezvous and docking laboratory on the international space station." *26th Annual AAS Guidance and Control Conf.*, Breckenridge, Colo.

Morton, B., and Weininger, N. (1999). "Collective management of satellite clusters." *AIAA Guidance, Navigation and Control Conf.*, Portland, Ore., 1576–1584.

Pan, H., and Kapila, V. (2001). "Adaptive nonlinear control for spacecraft formation flying with coupled translational and attitude dynamics." *IEEE Decision and Control Conf.*, Vol. 3, Orlando, Fla., 2057–2062.

Prussing, J. E., and Conway, B. A. (1993). *Orbital mechanics*, Oxford University Press, Oxford.

Redding, D. C., and Adams, N. J. (1989). "Linear-quadratic station keeping for the STS orbiter." *J. Guid. Control Dyn.*, 12(2), 248–255.

Robertson, A., Inalhan, G., and How, J. P. (1999). "Spacecraft formation flying control design for the Orion mission." *AIAA Guidance, Navigation and Control Conf.*, Portland, Ore.

Schaub, H., and Alfriend, K. T. (1999). "$J_2$ invariant relative orbits for

spacecraft formations." *Flight Mechanics Symp.*, NASA Goddard Space Flight Center, Greenbelt, Md.

Schaub, H., and Alfriend, K. T. (2000). "Hybrid Cartesian and orbit element feedback law for formation flying spacecraft." *AIAA Guidance, Navigation, and Control Conf.*, Denver.

Schaub, H., and Alfriend, K. T. (2001). "Impulsive feedback control to establish specific mean orbit elements of spacecraft formations." *J. Guid. Control*, 24(4), 739–745.

Schaub, H., Vadali, S. R., Junkins, J. L., and Alfriend, K. T. (2000). "Spacecraft formation flying control using mean orbit elements." *J. Astronaut. Sci.*, 48(1), 69–87.

Schiff, C., Rohrbaugh, D., and Bristow, J. (2000). "Formation flying in elliptical orbits." *IEEE Aerospace Conf.*, Vol. 7, Big Sky, Mont., 37–47.

Schweighart, S., and Sedwick, R. (2001). "A perturbative analysis of geopotential disturbances for satellite cluster formation flying." *IEEE Aerospace Conf.*, Vol. 2, Arlington, Va., 1001–1019.

Sedwick, R. J., Miller, D. W., and Kong, E. M. C. (1999). "Mitigation of differential perturbations in formation flying satellite clusters." *J. Astronaut. Sci.*, 47(3), 309–331.

Slotine, J. E., and Li, W. (1990). *Applied nonlinear control*, Prentice-Hall, Englewood Cliffs, N.J.

Ulybyshev, Y. (1998). "Long-term formation keeping of satellite constellation using linear-quadratic control." *J. Guid. Control Dyn.*, 21(1), 109–115.

Vadali, S. R., Schaub, H., and Alfriend, K. T. (1999). "Initial conditions and fuel optimal control for formation flying of satellites." *AIAA Guidance, Navigation, and Control Conf. and Exhibit*, Portland, Ore.

Vadali, S. R., Vaddi, S. S., and Alfriend, K. T. (2002). "An intelligent control concept for formation flying satellite constellations." *Int. J. Robust Nonlinear Control*, 12(2–3), 97–l15.

Vassar, R. H., and Sherwood, R. B. (1985). "Formation keeping for a pair of satellites in a circular orbit." *J. Guid. Control Dyn.*, 8(2), 235–242.

Wiesel, W. E. (2003). "Optimal impulsive control of relative satellite motion." *J. Guid. Control Dyn.*, 26(1), 74–48.

Xu, Y., and Fitz-Coy, N. (2003a). "Generalized relative dynamics and control in formation flying system." *26th Annual AAS Guidance and Control Conf.*, Breckenridge, Colo.

Xu, Y., and Fitz-Coy, N. (2003b). "Genetic algorithm based sliding mode control in the leader/follower satellites pair maintenance." *2003 AAS/AIAA Astrodynamics Specialist Conf.*, Big Sky, Mont.

Yan, Q., Kapila, V., and Sparks, A. G. (2000). "Pulse-based periodic control for spacecraft formation flying." *American Control Conf.*, Vol. 1, Chicago, 374–378.

Yedavalli, R. K., and Sparks, A. G. (2000). "Satellite formation flying control design based on hybrid control system stability analysis." *American Control Conf.*, Vol. 3, Chicago, 2210–2214.

Yen, H., Nelson, E., and Sparks, A. (2000). "Nonlinear tracking control for satellite formations." *Proc., 39th IEEE Conf. on Decision and Control*, Sydney, Australia, 328–333.